International Journal of Ocean System Engineering 1(2) (2011) 68-75
DOI 10.5574/IJOSE.2011.1.2.068

Edge Line Information based Underwater Landmark for UUV†

Son-Cheol Yu[1*], Dong-Joung Kang[2*] and Jaesoo Kim[3*]

[1]*POSTCH Ocean Science and Technology Institute, POSTECH, Pohang, Gyeonbuk 790-784, Korea*

[2]*School of Mechanical Engineering, Pusan National University, Busan 690-756, Korea*

[3]*Hanwha Corporation R&D Center, Daejeon 305-156, Korea*

(Manuscript Received February 23, 2010; Revised March 30, 2011; Accepted May 6, 2011)

Abstract

This paper addresses an underwater landmark for updating UUV positioning information. A method is proposed in which the landmark's cubic shape and edge are recognized. The reliability, installation load, and management of landmark design were taken into consideration in order to assess practical applications of the landmark. Landmark recognition was based on topological features. The straight line recognition confirmed the landmark's location and enabled an UUV to accurately estimated its underwater position with respect to the landmark. An efficient recognition method is proposed, which provides real-time processing with limited UUV computing power. An underwater experiment was conducted in order to evaluate the proposed method's reliability and accuracy.

Keywords: Underwater; Pose estimation; Position, UUV

1. Introduction

Unmanned underwater vehicles (UUV) automate risky underwater tasks such as monitoring underwater structures. Many underwater tasks will employ UUVs rather than manpower if the vehicle can automatically recognize a target object and precisely estimate the object's position. UUVs would improve the accuracy of the tasks as well as provide reliability with safety. Acoustic sensors have been used to achieve such accuracy and reliability. Acoustic beacons are examples of these sensors. They provide position with precision and high-reliability. However, they are expensive and possess high installation and management loads.

A passive man-made landmark located along a specific path serves as an alternative to active acoustic sensors. The man-made landmarks act as navigational aids, or serve as a zero position calibration devices that facilitate precision in underwater tasks. The landmark can be used to accurately localize the vehicle. In addition, landmarks enable UUVs to accomplish complicated tasks, such as underwater dexterous manipulation and the safety inspection of underwater structures.

Various UUV landmarks have been proposed. Maki proposed a floating pole acoustic landmark that guaranteed reliable detection over a long distance. The acoustic landmark could be detected from miles of distance.[3]. However, the floating acoustic landmark provides limited position variables (X,Y); thus, its application to actual UUVs is limited.

Park proposed a lighting lamp landmark for UUV docking [4]. Five strong lights were attached to a circular frame. These lights represented the landmark's feature points. This method extended the landmark's detecting range and improved the

†This paper was presented at the ISOPE 2009 conference, Osaka, Japan, 2009.

*Corresponding author. Tel.: +82-51-510-2356, Fax.: +82-51-510-2356.
E-mail address: djkang@pusan.ac.kr

Copyright © KSOE 2011.

reliability. However, the light assembly required a continuous support load, power supply and maintenance.

Yu proposed colored spheres that were attached to the landmark [5]. The spheres provided a wide range of detection (180 degrees) as well as reliability without excessive power consumption. There are 2 cues to detect the sphere. The one is the circle edge line and the other is the surface's color area of the sphere; the texture feature. However, if the spheres became covered with marine bio-fouling, the spheres lose both cues to detect. As a result, the spheres worked for only a short duration following installation.

The main function of the landmark design entails providing an accurate point of reference for the UUV using minimum support. With the actual UUV environments taken into consideration, the landmark should offer accurate position data using robust real-time recognition methods compatible with the UUV's small computing power. The landmark should not consume power and should be managed with minimum loading. Furthermore, and provide long term use under marine bio-fouling

2. Edge Line Information

Underwater landmarks can be recognized through two different methods: optical vision and acoustic. Optical vision provides the most accurate position data; however, its reliability is relatively lower than the reliability of an acoustic sensor, such as sonar. Conversely, the acoustic method exhibits lower accuracy with higher reliability.

Color extraction is the easiest method for optical vision when operating on land. Figure 1(a) shows an underwater cable image and Fig.1(b) shows its color distribution, which is quite concentrated. This method is efficient for short tem use because underwater environments typically exhibit monotonous backgrounds. However, marine bio-fouling is inevitable over long durations of use. Fig.2 shows the sacrificial anode [6] that protects underwater structures from rust. Fig.3 shows the covered sacrificial anode. Once the sacrificial anode was covered, all features of the anode's texture, namely its color, were lost.

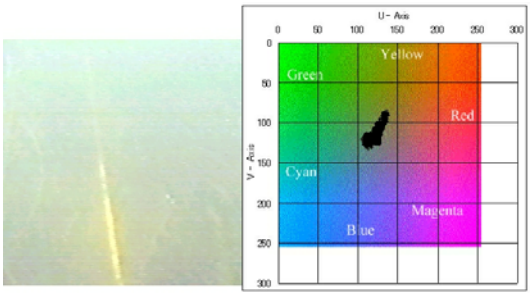

(a) Underwater Cable (b) Color Distribution in UV Space

Fig. 1. Underwater Cable Image

Fig. 2. Sacrificial Anode, Clean

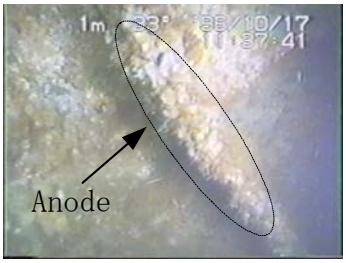

Fig. 3. Anode with Marine-Bio-Fouling

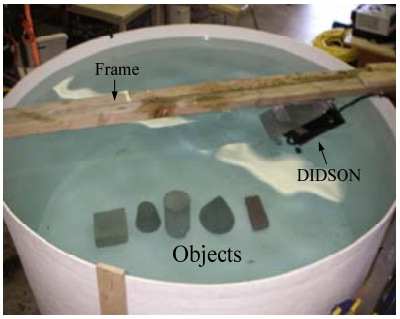

Fig. 4. Target Objects in Underwater

An alternative method to color extraction is using a straight line. The straight line compensates the shortcomings of the color extraction. The straight line method contributes to noise and marine bio-fouling. It is outstanding from the background; noise and marine bio-fouling. Usually, the background hardly has the lines. As shown in Fig.4, objects with various shapes were installed in an indoor water tank and their images were taken by a high-resolution sonar DIDSON [7][8]. Figures 5-8 show the images. Due to the sonar's acoustic nature and displaying mechanism [9], the concrete cylinder image differed from the optical image. Furthermore, edge line of the curvature differed from the actual edge. In Fig.6, the upper black triangle signifies the cone's shadow. The actual shadow is the highlighted upside down white triangle. Fig.7 shows a representative cube shape of a brick. Its shape corresponds with the optical image. The cubic consists of straight lines and is able to detect an object in underwater with a high degree of reliability.

We proposed a cube shaped landmark based on the characteristics described above. The object was recognized using the edges. Concrete proved to be a good candidate as the landmark's material. Concrete generates strong backscattering and it appears as a highly highlighted spot in the image, thus guaranteeing reliable detection. Reliable landmark shapes include concrete cubes and bricks [10][11]. The cube landmark is easy to build and install; therefore, the cube landmark is the practical solution.

UUVs can detect the landmark over a medium range using sonar. The UUVs are able to confirm the landmark's existence over a short range using the optical vision. Depending on the condition, either sensing method is available.

3. Camera Pose Estimation

Line based efficient object recognition was adopted as the recognition method of the landmark's lines [12][13].

The estimation of the landmark's position requires knowledge of the landmark's vertex and line intersections. However, floating particles often hide the lines, making the lines appear as dotted lines or short lengths underwater. The vertex may not be visible in the image. The proposed method locates the vertex by

Fig. 5. Concrete Cone (21(D)x25.5(H)cm)

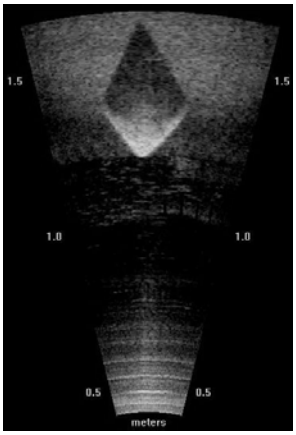

Fig. 6. Concrete Cylinder Image

Fig. 7. Brick (9.1x19.3x5.8(H)cm)

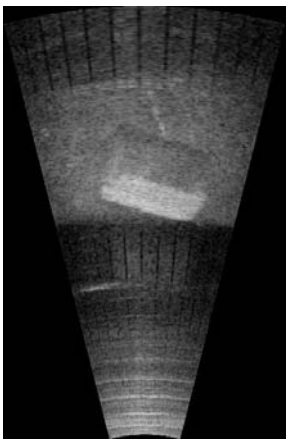

Fig. 8. Concrete Square Block

extending the extracted lines. It is independent to line length or status and efficiently calculates the vertex with high reliability. The proposed recognition has two stages:

1) Object recognition and Finding Correspondence.

Firstly, the AUVs detect the landmark. Lines are extracted from an image. Multiple lines must be grouped into the following categories: the target landmark and the background noise. However, grouping line junctions is a difficult task. This is related to energy model minimization necessary for efficiently finding the group.

The node relationships among the model's lines help characterize the relationship between the model and the detected object.

Let the model have *n* feature nodes. The sequential nodes generate a linked node chain. We can find the potential energy from the enumerated nodes when certain features are sequentially linked.

As an example, a pair of the model's lines correspond to the line features b_n, b_{n+1} in the image. If the relational configuration of each line node depends only on the connected *neighboring* nodes, the energy potential obtained from the *n* line nodes can be expressed as Eq. 1.

$$EP_{all}(b_1,b_2,...,b_n) = EP_1(b_1,b_2)+EP_2(b_2,b_3)+...+EP_{n-1}(b_{n-1},b_n) \quad (1)$$

Where,

$$EP_n(b_n,b_{n+1}) = \sum_{k=1}^{K} \left| q_{2,k}(b_n,b_{n+1}) - Q_{2,k}(n,n+1) \right| \quad (2)$$

The binary relations of a certain two connected line features in the image and the model are expressed as $q_{2,k}$ and $Q_{2,k}$, respectively. K is the number of the binary relations. The model junction and the corresponding junction in the image replace by the model and the image's node *n*, b_n in Eqs.1-2 for the relation representation.

Fig. 9 illustrates the edge line grouping method in a box type object. Sequentially connected junctions are used for the line pattern matching. Using this binary relation, Eq. 2 for the junction chains can be written as Eq.3.

$$EP_n(b_n,b_{n+1}) = \alpha \cdot \left| \theta(b_n) - \Theta(n) \right| + \beta \cdot \left| q(b_n,b_{n+1}) - Q(n,n+1) \right| \quad (3)$$

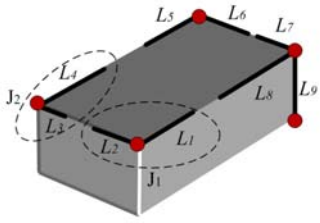

Fig. 9. Line Node Junctions Grouping

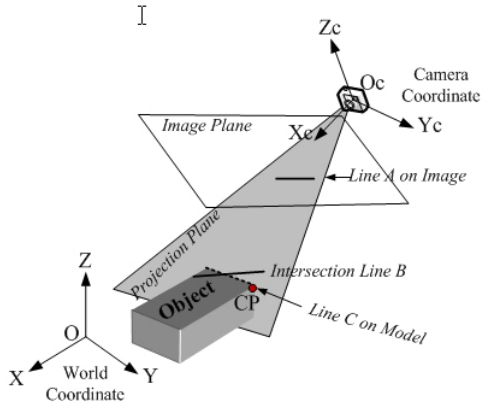

Fig. 10. Distance Measurements for Matching Evaluation

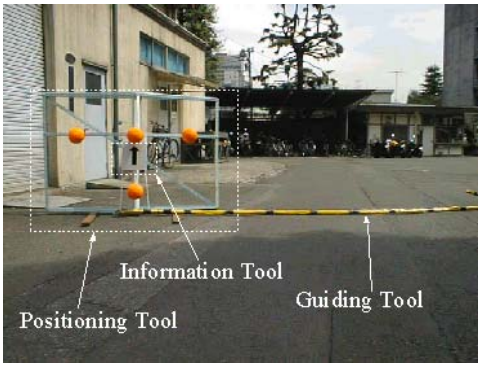

Fig. 11. Experimental Man-Made Underwater Landmark

Each junction has an *unary* angle relation formed by two lines constituting a single junction as shown in the first term of Eq. 4. $\theta(b_n)$ and $\theta(n)$ are the corresponding junction angles in the image and the model, respectively. The line's length is not considered for the recognition due to its uncertainty. In the Eq.(3), the binary relation for the image (q) and model (Q) is defined as a topological constraint or an angle relation between two junctions.

The cubic object is recognized using its topological characteristics. For example, the line pairs L1 and L4 or L2 and L7, are parallel. L1 and L2 are collinear and their junctions have a collinear constrain. Once energy potential is obtained from Eq.1, it is optimally minimized using DP (Dynamic Program) technique. Then a meaningful line group, the landmark, can be found with the correspondence of vertex with the 3D model.

2) Landmark position estimation and recognition

Using the correspondence, the landmark's relative position is estimated. The template is optimally modified for the recognition. It is matched with the acquired image for the final verification of the landmark.

Captured object images change depending on the camera view. If the 3D model of the object is known, we can predict the image at a certain position using perspective projection. If the cube landmark's position is perfectly estimated, the predicted wireframe image is exactly matched with the acquired wireframe from the actual image. The recognition's main issues are able to simplify just the edge line's detection and matching. In the cube's case, the edge lines are the wireframe of the cube. Kummar[14] dealt the wireframes' detection and matching issue, effectively.

We proposed a position estimation method that entailed solving rigid transformations, which minimizes the sum-of-squared distances between points of the 3-D model lines and the plane.

As shown in Fig.10, a camera and an object's coordinate systems are defined. The relationship between the two coordinate systems is given by the following vector-matrix Eq.4.

$$X_{p/Oc} = R^t \cdot (X_{p/Ow} - T_{p/Ow}) \tag{4}$$

where $\mathbf{R}$ is rotation matrix from the world coordinate system to the camera coordinate system and $\mathbf{T}_{o/o_w}=(t_1\ t_2\ t_3)^t$ is translation vector from O_w point to O_c point. Upper index t presents transpose of a matrix. A point in 3-D space is represented by the 3-D vector $\mathbf{P}$. Roll-pitch-yaw angles were used to represent the rotation matrix $\mathbf{R}$.

Due to the noise caused bey extraction image lines, the segments usually will not lie exactly in the projection plane as shown in Fig.10 The point-to-plane distance may be defined as the dot product of the unit normal to the plane and a 3-D point on the model line transformed to camera coordinates. It is possible to provide an error equation denoting the sum of squared perpendicular distances for line segments:

$$e = \sum_{i=1}^{l} \sum_{j=1}^{m} (\mathbf{N}_i \cdot (\mathbf{R}^t (\mathbf{P}_{ij} - \mathbf{T}))^2 \tag{5}$$

The summation is over l pairs of the corresponding 3-D and 2-D line segments. A point $\mathbf{P}$ on the 3-D model line in Fig. 10 might be one among two endpoints and center point of the line. The index m is the number of points selected on the 3-D line.

$\mathbf{N}_i$ is the unit normal vector to the plane formed by each 2-D segment. The pose of the 3-D segments relative to 2-D segments is expressed as a rotation $\mathbf{R}$ and translation $\mathbf{T}$ applied to the 3-D points. The best-fit 3-D pose for a set of corresponding 3-D and 2-D line segments is defined by the rotation $\mathbf{R}^*$ and translation $\mathbf{T}^*$ which minimize eq. 5. Solving for $\mathbf{R}^*$ and $\mathbf{T}^*$ is a non-linear optimization problem. It can be written for a specific point P on the 3-D model line as Eq.6.

$$e = \mathbf{N} \cdot \mathbf{R} \cdot (X - T) \tag{6}$$

where R is the rotational vector and T is the translation vector. N is the normal vector components of the plane obtained from the corresponding 2-D image line and 3-D model line. The $\mathbf{P}_{ij}$ with respect to the world coordinate system is $(X_{ij}\ Y_{ij}\ Z_{ij})^t$ and the translation vector $\mathbf{T}$ between two coordinate systems from O_w to O_c is given as $(t_1\ t_2\ t_3)^t$. The number of unknown parameters in eq. (6) is six for both $(t_1\ t_2\ t_3)$ of translation and $(\alpha\ \beta\ \gamma)$ of rotation.

From eq. (6), we can create an equation that expresses this error as the sum of the products of its partial de-

rivatives:

$$\frac{\partial e}{\partial t_1}\delta t_1+\frac{\partial e}{\partial t_2}\delta t_2+\frac{\partial e}{\partial t_3}\delta t_3+\frac{\partial e}{\partial \alpha}\delta\alpha+\frac{\partial e}{\partial \beta}\delta\beta+\frac{\partial e}{\partial \gamma}\delta\gamma=\delta e \quad (7)$$

For example, we can obtain six equations for three lines using two end points of a line and hence produce a complete linear system, which can be solved for all six camera-model corrections. In conventional cases, several line segments could give an over-constrained linear equation. The Levenberg-Marquardt method provides a solution for a linearized form of the non-linear equation. The small displacement vector $\delta\mathbf{x}$ including δt_1, δt_2, δt_3, $\delta\alpha$, $\delta\beta$, and $\delta\gamma$ represent errors of each parameter and define the Jacobian matrix $\mathbf{J}$. The partial derivatives of e with respect to each of the six parameters are analytically derived. The eq. (8) and (9) show an example of the partial derivatives.

$$\frac{\partial e}{\partial t_1}=-(n_1r_{11}+n_2r_{12}+n_3r_{13}) \quad (8)$$

$$\begin{aligned}\frac{\partial e}{\partial \alpha}&=n_1[(X_{ij}-t_1)\frac{\partial r_{11}}{\partial \alpha}+(Y_{ij}-t_2)\frac{\partial r_{21}}{\partial \alpha}+(Z_{ij}-t_3)\frac{\partial r_{31}}{\partial \alpha}]\\&+n_2[(X_{ij}-t_1)\frac{\partial r_{12}}{\partial \alpha}+(Y_{ij}-t_2)\frac{\partial r_{22}}{\partial \alpha}+(Z_{ij}-t_3)\frac{\partial r_{32}}{\partial \alpha}]\\&+n_3[(X_{ij}-t_1)\frac{\partial r_{13}}{\partial \alpha}+(Y_{ij}-t_2)\frac{\partial r_{23}}{\partial \alpha}+(Z_{ij}-t_3)\frac{\partial r_{33}}{\partial \alpha}]\end{aligned} \quad (9)$$

Therefore, Jacobian matrix is

$$\mathbf{J}=\left[\frac{\partial e}{\partial \alpha}\ \frac{\partial e}{\partial \beta}\ \frac{\partial e}{\partial \gamma}\ \frac{\partial e}{\partial t_1}\ \frac{\partial e}{\partial t_2}\ \frac{\partial e}{\partial t_3}\right]^t. \quad (10)$$

The Levenberg-Marquardt method is an iterative variation on the Newton method in non-linear estimation. The normal equations $\mathbf{H}\delta\mathbf{x}=\mathbf{J}^t\mathbf{J}\delta\mathbf{x}=\mathbf{J}^t\mathbf{e}$ are augmented to $\mathbf{H}'\delta\mathbf{x}=\mathbf{J}^t\mathbf{e}$ where $\mathbf{H}'=(1+\lambda\mathbf{I})\mathbf{H}$. The value λ is initialized to a small value. If the value obtained for $\delta\mathbf{x}$ reduces the error, the increment of $\mathbf{x}$ to $\mathbf{x}+\delta\mathbf{x}$ is accepted and λ is divided by 10 before the next iteration. On the other hand, if the error increases, then λ is multiplied by 10 and the augmented normal equations are solved again, until an increment that reduces the error is obtained.

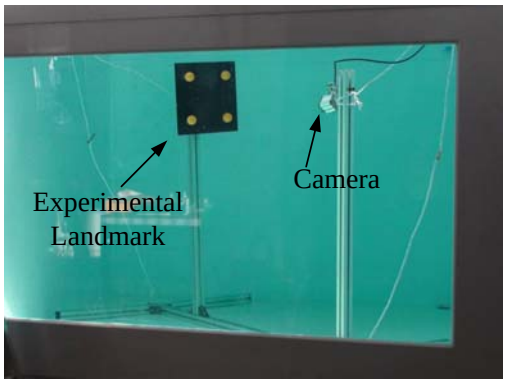

Fig. 12. Experimental Landmark Test Setup

Fig. 13. Raw Image, Result Overlapped

Fig. 14. Brick Image, Raw

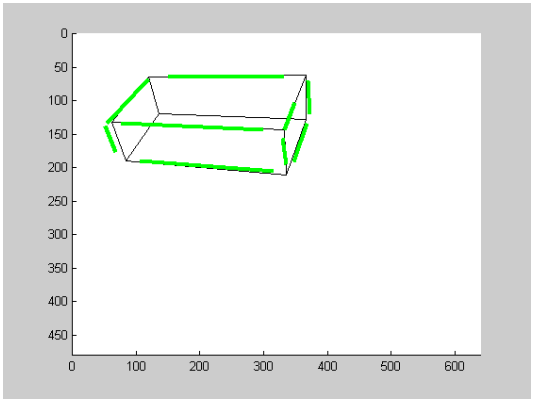

Fig. 15. Matching Result of Extracted Lines and 3D Model Lines, Image pixel frame

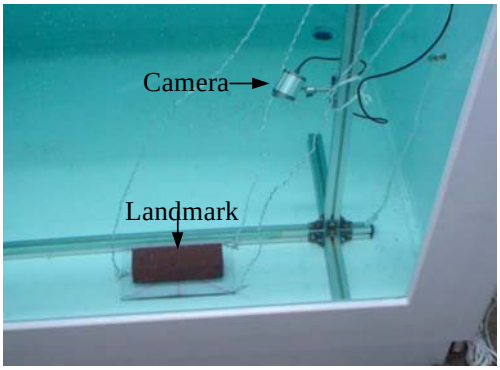

Fig. 16. Landmark Recognition Test Setup

Table 1. Position Estimation Result [cm, degrees]

Test	x	y	z	roll	pitch	yaw
1	-1.8	-1.6	0.1	0.8	0.3	1.6
2	-0.8	-1.1	0.7	0.5	1.2	0.8
3	0.6	0.5	0.5	0.8	0.3	0.4
4	-0.7	0.1	0.4	0.9	1.7	0.9
5	-2.8	-1.5	-0.2	0.2	0.8	1.3

Table 2. Brick's Position Estimation Result [cm, degrees]

Test	x	y	z	roll	pitch	yaw
1	1.7	2.3	0.7	0.8	1.4	0.4
2	2.5	2.5	0.9	0.5	2	0.4

Using the landmark position, 3D model is modified for the matching. The fit measurement error finally determines the landmark. If it is higher than the threshold, it is considered as the target landmark.

4. Experiment

On air and underwater tests were conducted in order to estimate the landmark's accuracy. The proposed method's estimated position accuracy and recognition reliability were evaluated. An experimental landmark was fabricated to evaluate the core part of the proposed landmark's detection and the proposed position estimation. As shown in Fig.11, spheres offer reliable point data underwater [5]. As shown in Fig.12, four colored spheres were attached to a plane on the vertex of the square.

A cubic has 4 junction points in each surface plane and the junction function represents the points. The sphere's diameter was 4 cm and the distance between two spheres was 18 cm. Using these known points, we found the camera parameter for underwater use. The parameters were $\alpha_u = 880.97$, $\alpha_v = 876.70, u_0 = 291.99, v_0 = 180.34$

As shown in Fig.16, the camera and the landmark were installed in the tank. A solid metal frame

As shown in Fig.13, the lines of the image were extracted and the target was recognized through the proposed calculation method. The landmark's X, Y, Roll, Pitch, and Yaw were fixed and the landmark only slid on Z-Axis. From 60 cm (Test1) to 100 cm (Test5), the Z values changed at 10 cm intervals. Table 1 shows the test results. The average position and the rotation angle error were about 0.9 cm and 0.8 degrees, respectively. These values exhibit good enough accuracy for UUV positioning and the landmark recognition.

The cubic landmark recognition test was tested in air. A brick (LxBxD, 23 x 11.5 x 6cm) was adopted as the landmark. Using the proposed recognition method, the edge lines were found and its position was estimated. Then, the acquired lines were matched with the brick's 3D CAD model at the found position. Fig.14 shows the raw image and Fig.15 illustrates the extracted lines from the image and 3D CAD Model at the estimated position. They matched well.

The estimated roll, pitch, and yaw angles were 16.8, -43.9, 10.9 degrees, respectively, and the XYZ positions were, -39.5,-10.1, and 32.7cm, respectively. The estimated straight lines were matched with the 3D model with a distance error of 0.04258[cm/line]. The result confirms the accuracy of the proposed method.

As shown in Fig.16, the brick's position estimation

test was carried out in tank. The brick was mounted on a scaled plate, indicating the position on the bottom. The relative x, y, z, roll, pitch, and yaw for Test1 and Test2 were (0,0,58cm,0,45,45 degrees) and (0,0,62,0,45,45), respectively. Table 2 shows the test results. The accuracy was lower due to error from the extracted line edges. The result showed good accuracy as the position reference underwater.

5. Conclusions

We proposed a reliable underwater landmark and recognition method for UUVs. The first stage of recognition entailed the line based camera pose estimation method. The line feature based landmark recognition was reliable for optical and acoustic sensing. The proposed recognition method was robust for underwater noise. The landmark design and recognition both accounted for underwater environments to improve reliability. In terms of system engineering, this approach can significantly improve the reliability of sensing.

The proposed line base object recognition is the initial stage of practical object recognition underwater. It has great potential to automate underwater tasks. Acoustic sonar based line feature recognition test will be planned as the next stage.

Acknowledgements

This research was supported by Hanwha Corporation R&D Center.

References

[1] J.K. Yuh, et. Al, *Design of a semi-autonomous underwater vehicle for interventionmissions (SAUVIM)*, Proc. of International symposium on Underwater Technology, (1998) 63-68.

[2] S.C. Yu, and T. Ura, *Experiment on a system of Multi-AUV Interlinked with a Smart Cable for Autonomous Inspection of Underwater Structures*, International J. of Offshore Structures and Polar Engineering, 14(4) (2004) 274-283.

[3] T. Maki, H. Kondo, T. Ura, T. Sakamaki, *Photo Mosaicing of Tagiri Shallow Vent Area by the AUV Tri-Dog 1 using a SLAM based Navigation Scheme*, Proc. of MTS/IEEE OCEANS CD-ROM, (2006).

[4] J.Y. Park, B.H. Jun, P.M. Lee, J. O, *Experiments on vision guided docking of an autonomous underwater vehicle using one camera*, Ocean Engineering, 36(1) (2009) 48-61.

[5] S.C. Yu, T. Ura, H. Fujii, H. Kondo, *Navigation of autonomous underwater vehicles based on artificial underwater landmarks*, MTS/IEEE OCEANS, l(1) (2001) 409-416.

[6] S.C. Yu, T. Ura and T. Samakaki, *Development of the New Recognition Method of Sacrificial Anodes and Navigation Method of AUVs for Automatic Inspection of Underwater Structures*, Proc.of Techno-Ocean International Symposium, CD-ROM T-D-2-1, (2002).

[7] DIDSON website, www.didson.com

[8] S. David, *The professional diver's handbook*, submex, U.K, (1982).

[9] T. Kazuo and T. Hmasahiro, *Fundamental of Oceanography*, Sanseido Press, (1997) 155-157 (in Japanese).

[10] S.C. Yu, *Development of real-time acoustic image recognition system using by autonomous marine vehicle*, Ocean Engineering, 35(1) (2008) 90-105.

[11] S.C. Yu, T.W. Kim, A. Asada, S. Weatherwax, B. Collins, J. Yuh, *Development of High-Resolution Acoustic Camera based Real-Time Object Recognition System by using Autonomous Underwater Vehicles*, Proc. of MTS/IEEE OCEANS, (2006) 1-6.

[12] D.J. Kang, J.E Ha, I.S. Kweon, *Fast object recognition using dynamic programming from combination of salient line groups*, Pattern Recognition, 36(1) (2003) 79-90.

[13] D.J. Kang, M. Jeong, *A Method for Camera Pose Estimation from Object of a Known Shape*, LECTURE NOTES IN CONTROL AND INFORMATION SCIENCES, 345 (2006) 606-613.

[14] R. Kumar, and A.R. Hanson, *Robust methods for Estimating Pose and a Sensitivity Analysis*, CVGIP: Image Understanding, 60 (1994) 313-342.